Pergamon

Int. J. Heat Mass Transfer. Vol. 40, No. 16, pp. 3827–3835, 1997

Printed in Great Britain
0017–9310/97 $17.00+0.00

PII: S0017–9310(97)00041–0

Solidification of ternary metal alloys—I. Model development

MATTHEW JOHN M. KRANE† and FRANK P. INCROPERA
Heat Transfer Laboratory, School of Mechanical Engineering, Purdue University, West Lafayette, IN 47907, U.S.A.

and

DAVID R. GASKELL
School of Materials Engineering, Purdue University, West Lafayette, IN 47907, U.S.A.

(*Received* 9 *February* 1996 *and in final form* 17 *January* 1997)

Abstract—Building on previous treatments of transport phenomena occurring during the solidification of binary alloys, a model is constructed to simulate the casting of ternary alloys. Specifically, the continuum mixture equations for the transport of mass, momentum, energy and species are modified to account for a third component. To close the model, supplemental thermodynamic relations, which are taken from the ternary equilibrium phase diagram and which treat the several primary solid phases, binary eutectic troughs, ternary eutectic and peritectic reactions and the formation of an intermetallic compound, are presented. Finally, a calculation procedure is developed for the thermodynamic model. Numerical results based on the application of this model are discussed in a companion paper [Krane and Incropera, *International Journal of Heat and Mass Transfer*, 1997, **40**, 3837–3847]. © 1997 Elsevier Science Ltd.

1. INTRODUCTION

During the solidification of metal alloys, several defects can arise which are influenced directly by the heat, mass and momentum transfers which occur during the process. One defect which has received considerable attention in recent years is the redistribution (or macrosegregation) of the various alloying components during freezing of an off eutectic mixture. In general, the components of an alloy freeze at different rates and over a temperature range, establishing thermal and solutal gradients which cause fluid motion and consequent macosegregation. In recent years, a significant amount of work has been done to model macrosegregation during alloy solidification and is reviewed in recent articles [1, 2].

One approach to modelling the behavior of a solidifying alloy uses a continuum formulation, which eliminates the need to explicitly track solidification fronts or to use artificial matching conditions at these fronts by modelling the entire domain with one set of equations. A common method uses classical mixture theory to derive, in terms of phase properties and phase mass fractions, advection–diffusion equations which describe the transport of mixture mass, momentum, energy and species, thereby eliminating the need for detailed descriptions of phase interactions [3–6].

While continuum mixture models have enjoyed a measure of success in at least qualitatively predicting the behavior of solidifying ingots, most applications have involved the solidification of binary alloys. While the study of binary mixtures is an obvious starting place, where one can examine a simple, well-defined system and more easily discern the basic transport phenomena involved in alloy casting, most commercially applicable alloys contain more than two components. In many cases, several of these components are only present in trace amounts and have small macroscopic effects. However, there are still many systems which have alloying elements in large enough quantities to significantly affect flow patterns and resulting macrosegregation.

The first analytical study of macrosegregation during the solidification of a multicomponent alloy was performed by Mehrabian and Flemings [7]. Their analysis developed a three component Scheil formulation for the partition of the components and invoked several simplifying assumptions, including prescribed solidification rates, a linear distribution of solid volume fraction and planar isotherms. Also, they ignored the effect of solidification at the invariant point, modelling only freezing on the primary liquidus surface and along the binary eutectic troughs. The velocity field which carried the solute-enriched fluid through the mushy zone was found from continuity, as the flow was driven entirely by shrinkage. The authors analyzed the effects of the initial composition and distance from the chilled surface on the formation

†Present address: School of Materials Engineering, Purdue University, West Lafayette, IN 47907, U.S.A.

NOMENCLATURE

B	specific buoyancy force [m s^{-2}]
c	specific heat [J kg^{-1} K^{-1}]
D	liquid mass diffusion coefficients [m^2 s^{-1}]
f	mass fraction
g	gravitational acceleration [m s^{-2}]
h	enthalpy [J]
h_f	heat of fusion [J kg^{-1}]
k	thermal conductivity [W m^{-1} K^{-1}]; equilibrium partition coefficient
K	permeability [m^2]
L	liquid phase
P	pressure [Nm^{-2}]
t	time [s]
T	temperature [K]
u	x-velocity [m s^{-1}]
v	y-velocity [m s^{-1}]
$\mathbf{V}$	velocity vector [m s^{-1}]
x, y	Cartesian coordinates [m].

Greek symbols

$\alpha, \beta, \gamma, \delta$	primary solid phases
β_s	solutal expansion coefficient
β_T	thermal expansion coefficient [1 K^{-1}]
μ	dynamic viscosity [kg s^{-1} m^{-1}]
ρ	density [kg m^{-3}].

Subscripts

BIN	binary trough
EUT	eutectic point
INV	invariant point (eutectic or peritectic)
l	liquid
LIQ	liquidus
m	mixture
PER	peritectic point
s	solid
SOL	solidus
T	thermal.

Superscripts

A, B, C	elements in ternary mixture.

of intermetallic compounds and primary phases of aluminium rich Al–Cu–Ni systems. General criteria developed for positive and negative segregation predict opposing segregation patterns for the Ni and Cu. This effect is due to the paths of the liquid compositions, which experience an overall increase in copper content in the liquid and a simultaneous decrease in nickel as solidification progresses. Because the melt was stably stratified (in these cases, the negative buoyancy due to copper enrichment of the liquid exceeded the positive buoyancy created by the nickel depletion), the flow was dominated by solidification shrinkage, which leads to the designated macrosegregation pattern. These predictions were confirmed by unidirectional solidification experiments on Al–Cu–Ni alloys chilled from below.

An improvement of the modelling of transport phenomena in multicomponent alloys is found in Fujii *et al.* [8]. This analysis, which examined the solidification of low carbon steel, was limited to the mushy zone, assumed planar fronts and did not account for coupled flow between the melt and the mushy zone. However, it did consider coupled temperature and composition fields. Also, the velocity field was found from a momentum equation based on D'Arcy's law and included both shrinkage and buoyancy effects. The authors based their thermodynamic model on the assumption that only the primary iron phase would form and that there would be no formation of secondary phases or intermetallics, which is an acceptable approximation for the steel alloys studied. They chose the change in liquid density across the mushy zone as a figure of merit and suggested minimizing this quantity with respect to composition in order to minimize macrosegregation.

The most recent study of macrosegregation in multicomponent alloys was published by Schneider and Beckermann [9], who calculated flow patterns, temperature fields and solute redistribution in two, five and ten component steel alloys. They expanded the continuum formulation derived in Ref. [1] to include several alloying elements and studied steel in which those elements combined to provide up to 1.8 wt% of the mixture (with the balance being Fe). These low concentrations of alloying constituents permitted the use of a thermodynamic model, similar to that of Fujii *et al.* [8], which assumed only primary Fe phase formation. This work is the first attempt to calculate macrosegregation in a multicomponent system, using a continuum model and including the full effects of buoyancy-induced flows. While some small local differences were present, overall macrosegregation patterns of the various solutes were found to be similar, as were some composition profiles across the solidified ingots. Because all of the alloying components were rejected into the liquid as the Fe-rich solid formed (only primary solidification was considered), all of the components were redistributed in a pattern representative of binary solidification. Flow in the mushy zone was in the direction of gravity, resulting in negative segregation at the top of the cavity and channels extending downward away from the chill wall. These trends are opposite to those predicted for a lead–tin alloy [10], which involved an ascending

interdendritic flow. While changing the number of components did not significantly affect the macrosegregation, Schneider and Beckermann [9] illustrated the importance of accurate thermodynamic data for predicting final solute redistribution. The results of simulations of solidification of the same 10 component steel with two different sets of data for partition coefficients and changes in liquidus temperature with composition showed opposite trends in macrosegregation. Finally, they found that the global extent of macrosegregation for the different components was linearly dependent on the equilibrium partition coefficient, which is to be expected at compositions which result in only primary solidification.

The purpose of the present work is to extend an existing binary alloy solidification model [4, 6] to a ternary system and to model the effects of thermosolutal convection. Although it is much less likely in low alloy steels, the formation of secondary and tertiary solid phases, including ternary eutectic and peritectic reactions, occurs in many commercially applicable metal alloys, such as superalloys and copper- or aluminium-based products, and may be treated using appropriate thermodynamic models. In this paper, the transport equations developed in Refs [4, 6] are modified to account for the effect of the third component. A discussion of possible solidification paths of a ternary alloy will follow, along with that of the corresponding closure model, which uses thermodynamic data taken from the ternary phase diagram. A companion paper [11] applies the general model to a specific ternary system (Pb–Sb–Sn) and discusses the resulting convective phenomena and solidification behavior.

2. TRANSPORT EQUATIONS

In previous works, transport equations for mixture mass, momentum, enthalpy and species were derived to model the solidification of binary alloys [4, 6]. These mixture quantities were defined as the linear combination of the corresponding phase quantities. In these definitions, all of the solid phases have been treated as a single phase, which is a reasonable approximation for the mixture momentum and enthalpy, if the solid phase densities and specific heats are close to one another.

In the calculation of phase compositions for binary alloys [12], the solid composition can be easily found from the solidus line, without reference to the individual solid phase fractions. However, for ternary systems, the compositions of the four solid phases are found at different sections of the solidus surface and must be calculated individually from phase diagram relations. The mixture composition of component A is, therefore, expressed as

$$f_{\mathrm{m}}^{\mathrm{A}} = f_\alpha f_\alpha^{\mathrm{A}} + f_\beta f_\beta^{\mathrm{A}} + f_\delta f_\delta^{\mathrm{A}} + f_\gamma f_\gamma^{\mathrm{A}} + f_{\mathrm{l}} f_{\mathrm{l}}^{\mathrm{A}}. \quad (1)$$

Similarly, for the second component, B, the mixture equation is

$$f_{\mathrm{m}}^{\mathrm{B}} = f_\alpha f_\alpha^{\mathrm{B}} + f_\beta f_\beta^{\mathrm{B}} + f_\delta f_\delta^{\mathrm{B}} + f_\gamma f_\gamma^{\mathrm{B}} + f_{\mathrm{l}} f_{\mathrm{l}}^{\mathrm{B}}. \quad (2)$$

Mass conservation requires $f_{\mathrm{m}}^{\mathrm{A}} + f_{\mathrm{m}}^{\mathrm{B}} + f_{\mathrm{m}}^{\mathrm{C}} = 1$, so a mixture equation for $f_{\mathrm{m}}^{\mathrm{C}}$ is not necessary.

The transport equations are derived by writing and summing separate mass, momentum, enthalpy and species balances for the solid and liquid phases, thereby eliminating phase interaction terms. To accommodate the use of standard numerical techniques [12], the mixture equations (except continuity) are then rewritten in the form of advection and diffusion terms for the mixture quantities. Applying a scaling analysis to eliminate negligible terms [13] and assuming a negligible effect of shrinkage [14] and solid particle transport on macrosegregation, the equations for mass, momentum, enthalpy and species transport are:

$$\frac{\partial \rho}{\partial t} + \frac{\partial}{\partial x}(\rho u_{\mathrm{m}}) + \frac{\partial}{\partial y}(\rho v_{\mathrm{m}}) = 0 \quad (3)$$

$$\frac{\partial}{\partial t}(\rho u_{\mathrm{m}}) + \nabla \cdot (\rho \mathbf{V}_{\mathrm{m}} u_{\mathrm{m}}) = \nabla \cdot \mu \nabla u_{\mathrm{m}} - \frac{\mu}{K_x} u_{\mathrm{m}} + \rho_{\mathrm{l}} B_x - \frac{\partial P}{\partial x} \quad (4)$$

$$\frac{\partial}{\partial t}(\rho v_{\mathrm{m}}) + \nabla \cdot (\rho \mathbf{V}_{\mathrm{m}} v_{\mathrm{m}}) = \nabla \cdot \mu \nabla v_{\mathrm{m}} - \frac{\mu}{K_y} v_{\mathrm{m}} + \rho_{\mathrm{l}} B_y - \frac{\partial P}{\partial y} \quad (5)$$

$$\frac{\partial}{\partial t}(\rho h_{\mathrm{m}}) + \nabla \cdot (\rho \mathbf{V} h_{\mathrm{m}}) = \nabla \cdot \left(\frac{k}{c} \nabla h_{\mathrm{m}}\right) + \nabla \cdot \left(\frac{k}{c} \nabla (h_{\mathrm{s}} - h_{\mathrm{m}})\right) - \nabla \cdot (\rho \mathbf{V} (h_{\mathrm{l}} - h_{\mathrm{m}})) \quad (6)$$

$$\frac{\partial}{\partial t}(\rho f_{\mathrm{m}}^{\mathrm{A}}) + \nabla \cdot (\rho \mathbf{V} f_{\mathrm{m}}^{\mathrm{A}}) = \nabla \cdot (\rho f_{\mathrm{l}} D_{\mathrm{l}} \nabla f_{\mathrm{m}}^{\mathrm{A}}) + \nabla \cdot (\rho f_{\mathrm{l}} D_{\mathrm{l}} \nabla (f_{\mathrm{l}}^{\mathrm{A}} - f_{\mathrm{m}}^{\mathrm{A}})) - \nabla \cdot (\rho \mathbf{V} (f_{\mathrm{l}}^{\mathrm{A}} - f_{\mathrm{m}}^{\mathrm{A}})). \quad (7)$$

Because the conservation equations are based on mixtures of phases (with all solid phases treated together), they remain substantially the same for an arbitrary number of components. Aside from additional supplemented thermodynamic relations discussed in Section 3, few alterations are needed to account for the third component in this study.

The first change is the addition of a second species transport equation, which describes the advection, diffusion and storage of the third element. Interdiffusion of the two alloying components will be neglected, relative to diffusion of the solutes in the primary component. While mixture mass fractions of the alloying elements may be small for systems of interest, this approximation could break down if the liquid compositions became large. However, because scaling analysis and supporting calculations reveal that solute diffusion in metal alloy solidification is generally a very small effect [13], results should not be sig-

nificantly influenced by neglecting interdiffusion. With this simplifying assumption, it is possible to use equation (7) with a second series transport equation,

$$\frac{\partial}{\partial t}(\rho f_{\mathrm{m}}^{\mathrm{B}}) + \nabla\cdot(\rho \mathbf{V} f_{\mathrm{m}}^{\mathrm{B}}) = \nabla\cdot(\rho f_{\mathrm{l}} D_{\mathrm{l}} \nabla f_{\mathrm{m}}^{\mathrm{B}}) + \nabla\cdot(\rho f_{\mathrm{l}} D_{\mathrm{l}} \nabla(f_{\mathrm{l}}^{\mathrm{B}} - f_{\mathrm{m}}^{\mathrm{B}})) - \nabla\cdot(\rho \mathbf{V}(f_{\mathrm{l}}^{\mathrm{B}} - f_{\mathrm{m}}^{\mathrm{B}})) \quad (8)$$

to compute the mixture composition.

The buoyancy terms of equations (4) and (5) include both thermal and solutal effects, which are proportional to the differences between local and initial values of temperature and liquid solute concentrations, respectively. Including the effect of the third component and using a coordinate system with gravity antiparallel to the y-axis, the buoyancy terms in equations (4) and (5) can be written as

$$B_x = 0 \quad (9)$$

and

$$B_y = g\beta_{\mathrm{T}}(T - T_0) + g\beta_{\mathrm{S}}^{\mathrm{A}}(f_{\mathrm{l}}^{\mathrm{A}} - f_{\mathrm{l},0}^{\mathrm{A}}) + g\beta_{\mathrm{S}}^{\mathrm{B}}(f_{\mathrm{l}}^{\mathrm{B}} - f_{\mathrm{l},0}^{\mathrm{B}}). \quad (10)$$

The last two terms in equation (10) represent the contributions to the buoyancy force of both alloying elements. The thermal and solutal expansion coefficients are

$$\beta_{\mathrm{T}} = -\frac{1}{\rho}\frac{\partial \rho_{\mathrm{l}}}{\partial T} \quad \text{and} \quad \beta_{\mathrm{S}}^{i} = -\frac{1}{\rho}\frac{\partial \rho_{\mathrm{l}}}{\partial f_{\mathrm{l}}^{i}} \quad (i = \mathrm{A}, \mathrm{B}) \quad (11)$$

respectively.

Using standard procedures [12], the transport equations may be solved for the mixture velocities, enthalpy and species mass fractions. However, solutions explicitly depend on the temperature and the phase compositions and fractions. In the next section, it will be shown how, given the mixture enthalpy and composition $(h_{\mathrm{m}}, f_{\mathrm{m}}^{\mathrm{A}}, f_{\mathrm{m}}^{\mathrm{B}})$ found by the solution of equations (3)–(8), the ternary phase diagrams can be used to generate these values.

3. THERMODYNAMIC CLOSURE MODEL

3.1. *Solidification paths*

Before describing the method of obtaining the supplemental relations needed to close the continuum model, a short discussion of the solidification paths in a three component system will be given, aided by an idealized ternary phase diagram. More complete information concerning the use of these types of diagrams is given in [15–16].

A ternary equilibrium phase diagram is generally represented by a triangular prism, with temperature as the axial coordinate and composition represented on the base, which is an equilateral triangle. The three vertical sides of the prism are the three binary phase diagrams formed by the three combinations of the components. Figure 1 shows a top view of an idealized ternary phase diagram for the elements A, B and C, where the dotted lines are isotherms on the liquidus surface and the solid lines are paths of binary solidification. There is an intermetallic compound (X) on the AC diagram, which also has binary eutectic (e_{AX}) and peritectic (p_{CX}) points. The systems AB and BC have simple binary diagrams with eutectic points at

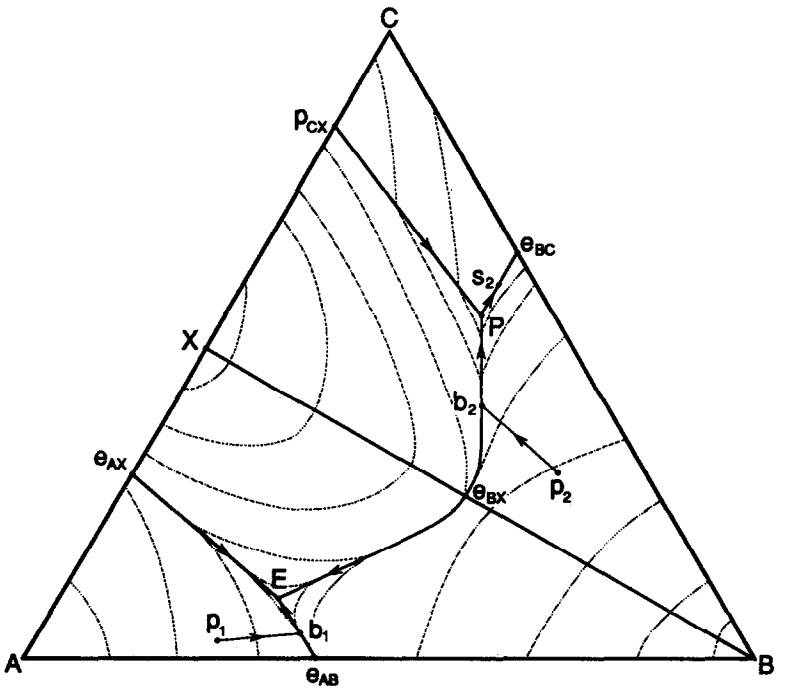

Fig. 1. Projection of liquidus surface of idealized ternary phase diagram for ABC system.

e_{AB} and e_{BC}, respectively. The interior of the three component diagram shows some features of the liquidus surface. The quasibinary system BX, with its binary eutectic, e_{BX}, is indicated, as are the binary troughs (or valleys), such as $[e_{BC}P]$, and the ternary invariant points, E(eutectic) and P (peritectic).

While considering the solidification process, it is useful to recall Gibbs' phase rule. If one selects a constant pressure at which the system is examined, for a ternary alloy this rule is reduced to

$$F = 4 - \Phi \tag{12}$$

where Φ is the number of phases and F the degrees of freedom.

At temperatures above the liquidus surface shown in Fig. 1, the mixture is completely liquid ($\Phi = 1$) and $F = 3$, the maximum value. Temperature and composition can be changed within a specified volume without changing phase. As the temperature is lowered at a constant mixture composition, the liquidus surface is encountered (for example, at $[p_1]$ in Fig. 1) and primary solidification begins. Solidification involves the primary crystallization of an A-rich α solid solution from the melt and a consequent change in the composition of the liquid over the liquidus surface along the path $[p_1b_1]$. In this case, $F = 2$ and the possible states are limited to two dimensional surfaces. When the liquid composition reaches a binary trough $[e_{AB}E]$ at $[b_1]$, the liquid becomes saturated with a B-rich β solid solution and further heat removal from the system causes secondary crystallization of α and β from the doubly-saturated liquid ($L \rightleftarrows \alpha + \beta$). With three phases present, $F = 1$ and each temperature uniquely determines the compositions of the three phases. With further decrease in temperature, the composition of the liquid moves down the binary saturated trough $[e_{AB}E]$. At the ternary eutectic temperature, the liquid composition reaches point E and the liquid becomes saturated with the solid solution δ, which is the primary solid solution of the intermetallic compound X. From equation (12), with $\Phi = 4$, $F = 0$ and, thus, the four-phase equilibrium exists only at the ternary eutectic temperature. Further heat removal causes isothermal decomposition of the melt of fixed composition E to form ternary eutectic α, β and δ solid phases, also of fixed compositions, according to $L \rightleftarrows \alpha + \beta + \delta$.

Another possible solidification path, $[p_2b_2Ps_2]$, is indicated on Fig. 1. The primary and secondary solidification ($[p_2b_2]$ and $[b_2P]$, respectively) proceed in a manner similar to that described for $[p_1b_1E]$. However at the invariant point P, the composition of the liquid lies outside the triangle formed by the compositions of the β, γ and δ phases with which it is in equilibrium. Thus the invariant reaction which occurs at P is a peritectic, which involves isothermal reaction of the liquid with the δ phase to form β and γ ($L + \delta \rightleftarrows \beta + \gamma$). If the liquid is depleted first, the freezing process is completed at the peritectic temperature. However, if the δ phase is depleted first, continued heat removal causes binary crystallization of β and γ from the melt. The liquid composition moves down the binary trough $[Pe_{CB}]$ and the last liquid disappears at some point $[s_2]$ in this trough.

3.2. *Primary solidification*

In the foregoing general description of possible solidification paths, the primary solidification was described as a region in which one solid phase is in thermodynamic equilibrium with the liquid, $L \rightleftarrows \alpha$. In this case, the mixture enthalpy and species definitions and mass conservation are:

$$h_m = f_l(c_l T + h_l^0) + f_\alpha(c_S T) \tag{13}$$

$$f_\alpha + f_l = 1 \tag{14}$$

$$f_m^A = f_\alpha f_\alpha^A + f_l f_l^A \tag{15}$$

and

$$f_m^B = f_\alpha f_\alpha^B + f_l f_l^B \tag{16}$$

where $h_l^0 = (c_s - c_l)T_{SOL} + h_f$.

In Fig. 2(a), the two phase ($\alpha + L$) region is seen in an isothermal section of the phase diagram shown in Fig. 1. The temperature is not known *a priori*, except that it is between the appearances of the first primary solid phase (at T_{LIQ}) and the first secondary solid phase (at T_{BIN}) for the mixture composition (f_m^A, f_m^B). Examining equations (13)–(16), there are four equations and seven unknown ($T, f_\alpha, f_l, f_\alpha^A, f_\alpha^B, f_l^A, f_l^B$), where h_m, f_m^A and f_m^B are found by the solution to equations (3)–(8).

Two more equations can be provided by the definition of the equilibrium partition coefficients, k_α^A and k_α^B, which are physical properties relating the compositions of the liquid and solid at equilibrium.

$$k_\alpha^j = f_\alpha^j / f_l^j \quad (j = A, B). \tag{17}$$

In general, these coefficients will be functions of temperature and mixture composition. The final relation needed to solve for the temperature and the phase fractions and compositions corresponds to the shape of the liquidus surface, which can be written as temperature as a function of liquid composition

$$T = T_{LIQ}(f_l^A, f_l^B). \tag{18}$$

This function is well-known for most common ternary systems.

3.3. *Secondary solidification*

When the liquid composition in Fig. 2(a) reaches a binary trough (e.g. at point $[b_1]$), a second solid phase begins to precipitate and a three phase equilibrium is established, $L \rightleftarrows \alpha + \beta$. Figure 2(b) shows an isothermal section of the ternary diagram between the temperature at $[b_1]$, T_{BIN}, and the eutectic temperature, T_{EUT}. If $T_{BIN} > T > T_{EUT}$, the liquid composition is known as a function of temperature:

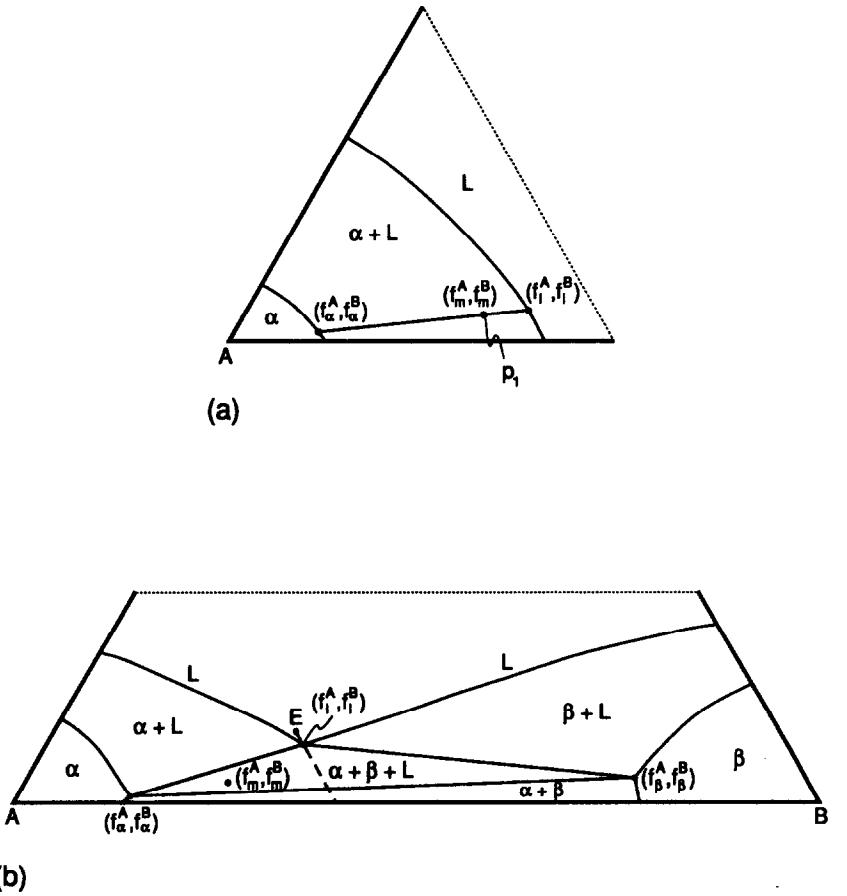

Fig. 2. (a) Isothermal section of A corner of Fig. 1, at $T_{LIQ} < T < T_{BIN}$; (b) isothermal section of A and B corners of Fig. 1, at $T_{BIN} < T < T_{EUT}$.

$$f_l^j = f_{l,BIN}^j(T) \quad (j = A, B). \tag{19}$$

These are the equations which prescribe the binary eutectic trough, as shown by the dashed line in Fig. 2(b). As the temperature drops further towards T_{EUT}, the liquid composition moves towards point E on the diagram. With the liquid compositions known as functions of temperature, the solid phase compositions may be found from knowledge of the equilibrium partition coefficients. As from equations (17), the solid phase compositions for β can be found:

$$f_B^j = k_\beta^j f_l^j \quad (j = A, B) \tag{20}$$

Finally, equations (13)–(16), respectively, are rewritten for the $L \rightleftarrows \alpha + \beta$ equilibrium regime.

$$h_m = f_l(c_l T + h_l^0) + (f_\alpha + f_\beta)(c_S T) \tag{21}$$

$$f_\alpha + f_\beta + f_l = 1 \tag{22}$$

$$f_m^A = f_\alpha f_\alpha^A + f_\beta f_\beta^A + f_l f_l^A \tag{23}$$

$$f_m^B = f_\alpha f_\alpha^B + f_\beta f_\beta^B + f_l f_l^B. \tag{24}$$

Equations (17) and (19)–(24) are sufficient to find the ten unknowns $(T, f_\alpha, f_\beta, f_l, f_\alpha^A, f_\alpha^B, f_\beta^A, f_\beta^B, f_l^A, f_l^B)$.

3.4. *Invariant points*

Both solidification paths in Fig. 1 contain invariant four-phase equilibria involving a liquid and three solid phases. At the eutectic point (E), isothermal solidification of the melt produces three solid phases (α, β and δ) of fixed compositions, while, at the peritectic point (P), liquid of composition P reacts with the δ phase to produce β and γ.

As seen in Fig. 3, which is an isothermal section of the ABX system at the eutectic temperature, T_{EUT}, there is a three phase triangle which includes the point E. The temperature and the liquid compositions are known and the solid compositions can be found using equations (17), (20) and

$$f_\delta^j = k_\delta^j f_l^j \quad (j = A, B). \tag{25}$$

The mixed relations needed to close the model for the eutectic reaction ($L \rightleftarrows \alpha + \beta + \delta$) are

$$h_m = f_l(c_l T_{EUT} + h_l^0) + (f_\alpha + f_\beta + f_\delta)(c_S T_{EUT}) \tag{26}$$

$$f_\alpha + f_\beta + f_\delta + f_l = 1 \tag{27}$$

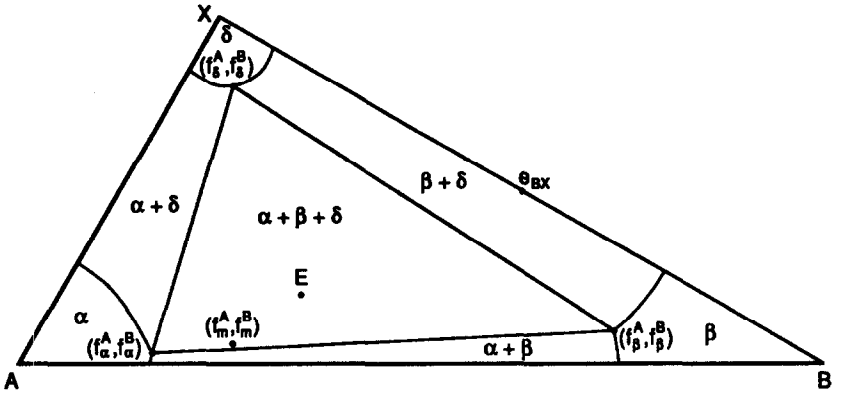

Fig. 3. Isothermal section of ABX system, at $T = T_{EUT}$.

$$f_m^A = f_\alpha f_\alpha^A + f_\beta f_\beta^A + f_\delta f_\delta^A + f_l f_l^A \quad (28)$$

$$f_m^B = f_\alpha f_\alpha^B + f_\beta f_\beta^B + f_\delta f_\delta^B + f_l f_l^B. \quad (29)$$

During the eutectic reaction, the liquid is partitioned so that the three solid phases are produced at the same rate. The peritectic reaction which occurs at point $P(L + \delta \rightleftarrows \beta + \gamma$, where γ is the primary solid phase of element C) does not have such a partition. As the temperature approaches T_{PER}, the liquid composition approaches P along either of two binary troughs, $[p_{CX}P]$ or $[e_{BX}P]$. If the liquid composition follows the $[p_{CX}P]$ trough, three phases (δ, γ and the liquid) would be present. If solidification proceeds down the $[e_{BX}P]$ valley, the β, δ and liquid phases would be present as T_{PER} is reached. During the peritectic reaction, the compositions of the four phases and the temperature do not change; only the relative amounts of the phases are altered by the freezing. The reaction freezes the liquid into β and γ phases, into which the δ solid is also transformed.

Knowing $T = T_{PER}$ and the liquid composition and using

$$f_i^j = k_i^j f_l^j \quad (j = A, B; i = \beta, \gamma, \delta) \quad (30)$$

to find the solid compositions, the mixture relations needed to close the model for the peritectic reaction are

$$h_m = f_l(c_l T + h_l^0) + (f_\beta + f_\gamma + f_\delta)(c_S T) \quad (31)$$

$$f_\beta + f_\gamma + f_\delta + f_l = 1 \quad (32)$$

$$f_m^A = f_\beta f_\beta^A + f_\gamma f_\gamma^A + f_\delta f_\delta^A + f_l f_l^A \quad (33)$$

$$f_m^B = f_\beta f_\beta^B + f_\gamma f_\gamma^B + f_\delta f_\delta^B + f_l f_l^B \quad (34)$$

4. CALCULATION PROCEDURE

In the previous sections, transport equations were developed for the calculation of mixture velocities, enthalpy and two species mass fractions. Using the values for enthalpy and composition, thermodynamic models, based on mixture relations and a ternary phase diagram, were derived for solidification in the primary region, binary troughs and two kinds of invariant points. In order to use these models to calculate temperature and phases compositions and fractions, two related pieces of information are needed. The value of the solidus temperature, T_{SOL}, is needed to find the temperature from the mixture enthalpy and a determination must be made of the region in which solidification is occurring.

For each mixture composition, there is a unique solidification path, such as the two paths discussed earlier. However, the two examples are extreme in the sense that they pass through all possible types of regions in the phase diagram. Depending on the mixture composition, solidification may not terminate necessarily at the end of these curves and T_{SOL} may be higher than the temperatures at the end of the designated paths. The first step in determining T_{SOL} is to find out in which region of the phase diagram (primary, binary trough, or invariant point) solidification ends. To this end, the mass fraction of liquid remaining at several control points along a possible path will be calculated. These control points are the beginning of binary solidification and the beginning and the end of the invariant reactions.

At the transition point between primary solidification and a binary trough (e.g. $[b_l]$), $f_\beta = 0$ and the phase compositions and fractions $(f_\alpha, f_l, f_\alpha^A, f_\alpha^B, f_l^A, f_l^B)$ can be calculated from equations (13), (15)–(17) and

$$f_l^A = f_{l,BIN}(f_l^B). \quad (35)$$

Equation (35) describes the path of the binary trough as projected on the base of the phase diagram and can be obtained by eliminating temperature from equations (19). If the liquid fraction calculated at this point, $f_{l,BIN}$ is less than zero, solidification ends with only α phase formation. The solidus temperature can then be found by using $f_\alpha = 1$ and $f_m^i = f_\alpha^i (i = A, B)$ with equations (17) and (18) to obtain

$$T_{SOL} = T_{LIQ}(f_m^A/k_\alpha^A, f_m^B/k_\alpha^B). \quad (36)$$

If $f_{l,BIN} > 0$, some liquid survives to freeze along the binary valley. The next control point is the state at which that valley ends in an invariant point, *before*

Table 1. Equations for calculating phase fractions and compositions and temperature during the various stages of solidification

$h_{LIQ} < h$	liquid	$f_l = 1$, $T = (h_m - h_l^0)/c_l$
$h_{BIN} < h < h_{LIQ}$	primary solidification	solve equations (13)–(18) for $T, f_\alpha, f_l, f_\alpha^A, f_l^A, f_\alpha^B, f_l^B$
$h_{INV} < h < h_{BIN}$	binary trough	solve equations (17), (19)–(24) for $T, f_\alpha, f_\beta, f_l, f_\alpha^A, f_\beta^A, f_l^A, f_\alpha^B, f_\beta^B, f_l^B$
$h_{SOL} < h < h_{INV}$	eutectic reaction	solve equations (17), (20), (25)–(29) for $f_\alpha, f_\beta, f_\delta, f_l, f_\alpha^A, f_\beta^A, f_\delta^A, f_\alpha^B, f_\beta^B, f_\delta^B$
$h_{PER} < h < h_{INV}$	peritectic reaction	solve equations (30)–(34) for $f_\gamma, f_\beta, f_\delta, f_l, f_\gamma^A, f_\beta^A, f_\delta^A, f_\gamma^B, f_\beta^B, f_\delta^B$
$h_{SOL} < h < h_{PER}$	binary trough following peritectic	replacing α with γ, solve equations (17), (19)–(24) for $T, f_\gamma, f_\beta, f_l, f_\gamma^A, f_\beta^A, f_l^A, f_\gamma^B, f_\beta^B, f_l^B$
$h < h_{SOL}$	solid	$f_l = 0$, $T = h_m/c_s$

the formation of the third solid phase. There, the temperature (T_{INV}) and the liquid composition ($f_{l,INV}^A, f_{l,INV}^B$) are known from the phase diagram. The remaining phases fractions and compositions ($f_\alpha, f_\beta, f_l, f_\alpha^A, f_\alpha^B, f_\beta^A, f_\beta^B$) can be found using equations (17), (20), (21), (23) and (24). The corresponding mass fraction liquid $f_{l,INV}$, represents the residual liquid existing when the third solid phase begins to form. If $f_{l,INV} < 0$ (and $f_{l,BIN} > 0$), freezing is complete somewhere along the binary trough. To find T_{SOL} along that valley, equations (17) and (19)–(21), as well as equations (23)–(24) (with $f_l = 0$), are solved simultaneously for $T_{SOL}, f_\alpha, f_\beta, f_\alpha^A, f_\alpha^B, f_\beta^A, f_\beta^B, f_l^A$ and f_l^B.

If there is liquid left at the beginning of the invariant reaction ($f_{l,INV} > 0$), the liquid fraction at the end of this reaction must be checked. For eutectic solidification, no liquid remains and $T_{SOL} = T_{EUT}$, which is known from the phase diagram. For the peritectic reaction, some liquid may remain, with the solidification continuing and the liquid composition running down a binary trough to lower temperatures. To find out if this is the case, it is assumed that $f_\delta = f_\delta^A = f_\delta^B = 0$ and equations (30), (31), (33) and (34) are solved for $f_\beta, f_\gamma, f_l, f_\beta^A, f_\beta^B, f_\gamma^A$ and f_γ^B. If f_l ($= f_{l,PER}$) is less than zero, the peritectic reaction ($L + \delta \rightleftarrows \beta + \gamma$) consumed the liquid before the δ solid and the solidification ends at $T_{SOL} = T_{PER}$. If $f_{l,PER} > 0$, T_{SOL} is found in the following binary trough in the manner described above.

The preceding procedure yields the solidus temperature, and the liquid mass fractions and temperatures at the control points between the solidification regimes described in Section 3. With all of the information needed to close the model, the only remaining requirement is to determine the applicable regime for calculating the temperature and the phase fractions and compositions. The mixture enthalpy at the control points for a given mixture composition can be calculated:

$$h_{LIQ} = c_l T_{LIQ} + h_l^0 \tag{37}$$

$$h_{BIN} = f_{l,BIN}(c_l T_{BIN} + h_L^0) + (1 - f_{l,BIN})(c_s T_{BIN}) \tag{38}$$

$$h_{INV} = f_{l,INV}(c_l T_{INV} + h_L^0) + (1 - f_{l,INV})(c_s T_{INV}) \tag{39}$$

$$h_{PER} = f_{l,PER}(c_l T_{PER} + h_L^0) + (1 - f_{l,PER})(c_s T_{PER}) \tag{40}$$

$$h_{SOL} = c_s T_{SOL}. \tag{41}$$

These enthalpies correspond to the beginning of the primary solidification (37), the intersection of primary liquidus surface and the binary trough (38) and the transition from binary freezing to the invariant reaction (39). Equation (4) is the enthalpy at the end of the peritectic reaction and h_{SOL} is the mixture enthalpy when the last liquid disappears. It should be noted that all possible solidification paths on a ternary phase diagram include h_{SOL} and h_{LIQ}, but whether the other control points apply to a particular path depends on the mixture composition found by solution to the transport equations. If solidification ends before a particular control point is reached, the corresponding enthalpy is not considered.

For these control enthalpies, $h_{SOL} < h_{PER} < h_{INV} < h_{BIN} < h_{LIQ}$. Once these values are calculated, they are compared to the mixture enthalpy found by solving equations (3)–(8) in order to determine the solidification regime. The appropriate methods of determining phase compositions and fractions, as well as temperature, are listed in Table 1. When using this table, one must keep in mind that the solid phases used in the equations assume the solidification paths from Fig. 1. If other mixture compositions are used, the paths and possibly the pertinent solid phases, will differ, but the methodology is the same.

5. SUMMARY

Building on previous models of mass, momentum, energy and species transport in binary alloys, a model has been developed to simulate the solidification of ternary alloys. The continuum mixture equations of this study are substantially the same as those for a binary alloy [4, 6], differing only in the buoyancy terms and the addition of a second species equation.

This set of transport equations (3–8) can be solved to find local values of mixture velocities, enthalpy and composition, which, in turn, are used to find temperature and phase composition and fraction fields through a thermodynamic closure model (Table 1).

The closure model is based on the ternary equilibrium phase diagram. The use of this type of diagram for multicomponent systems presents modelling problems which do not arise in the use of binary diagrams. One of the main concerns is that the solidus surface and the tie lines connecting it to the liquidus surface are not well characterized for almost all real systems. Because such detailed data are rarely available, the solidus surface is found using equilibrium partition coefficients. These property data are frequently approximated as constants with prescribed values equal to those of the associated binary diagram. This approximation is generally valid for alloys with few components (less than 4 or 5) or at low concentrations.

Another difficulty with the use of the ternary phase diagram is the assumption of thermodynamic equilibrium. Because temperature differences between solid and liquid phases are small over length scales corresponding to dendritic arm spacings, thermal equilibrium is an acceptable approximation. However, species diffusion in the solid is slow relative to conduction, calling into question the assumption of compositional equilibrium. While the inapplicability of this assumption may have only minor effects on the redistribution of the alloying elements, as suggested by a study of a binary alloy [10], it might cause significant deviations in the prediction of solid phase functions. This problem is particularly important during the ternary peritectic reaction, which assumes that one solid phase is transformed into two others. Although such solid–solid transformations tend to be slow compared to the time scales of the solid–liquid reactions, the proposed model assumes rapid phase change.

The transport equations, thermodynamic closure model and calculation procedures developed in this paper can be used to simulate the transport phenomena and solidification behavior during the casting of ternary alloys which have phase diagram features such as binary eutectic troughs, intermetallic compounds and ternary eutectic and peritectic points. This model is applied to a three component system (Pb–Sb–Sn) in a companion paper [11], in which binary and ternary macrosegregation are compared and contrasted and in Ref. [17], which includes an expanded discussion of [11] and further numerical results.

Acknowledgements—The authors would like to thank the Department of Energy for support of this research through Award Number DE-FG02-87ER13759.

REFERENCES

1. Beckermann, C. and Viskanta, R., Mathematical modeling of transport phenomena during alloy solidification. *Applied Mechanics Review*, 1993, **46,** 1–27.
2. Prescott, P. J. and Incropera, F. P., Convective heat and mass transfer in alloy solidification. In *Advances in Heat Transfer*, Vol. 28. ed. J. P. Hartnett, T. Irvine, Jr, Y. I. Cho and G. A. Green. Academic Press, New York, 1996, pp. 231–238.
3. Voller, V. P. and Prakash, C., A fixed-grid numerical modelling methodology for convection–diffusion mushy region phase-change problems. *International Journal of Heat and Mass Transfer*, 1987, **30,** 1709–1719.
4. Bennon, W. D. and Incropera, F. P., A continuum model for momentum, heat and species transport in binary solid–liquid phase change systems—I. Model formulation. *International Journal of Heat and Mass Transfer*, 1987, **30,** 2161–2170.
5. Amberg, G., Computation of macrosegregation in an iron–carbon cast. *International Journal of Heat and Mass Transfer*, 1991, **34,** 217–227.
6. Prescott, P. J., Incropera, F. P. and Bennon, W. D., Modelling of dendritic solidification systems: reassessment of the continuum momentum equation. *International Journal of Heat and Mass Transfer*, 1991, **34,** 2351–2359.
7. Mehrabian, R. and Flemings, M. C., Macrosegregation in ternary alloys. *Metallurgical Transactions*, 1970, **1,** 455–464.
8. Fujii, T., Poirier, D. R. and Flemings, M. C., Macrosegregation in a multicomponent low alloy steel. *Metallic Transfer B*, 1979, **10B,** 331–339.
9. Schneider, M. C. and Beckermann, C., Formation of macrosegregation by multicomponent thermosolutal convection during solidification of steel. *Metallurgical and Materials Transactions A*, 1995, **26A,** 2373–2388.
10. Schneider, M. C. and Beckermann, C., A numerical study of the combined effects of microsegregation, mushy zone permeability and flow, caused by volume contraction and thermosolutal convection, on macrosegregation and eutectic formation in binary alloy solidification. *International Journal of Heat and Mass Transfer*, 1995, **38,** 3455–3473.
11. Krane, M. J. M. and Incropera, F. P., Solidification of ternary metal alloys—II. Predictions of convective phenomena and solidification behavior in Pb–Sb–Sn alloys. *International Journal of Heat and Mass Transfer*, 1997, **40,** 3837–3847.
12. Bennon, W. D. and Incropera, F. P., Numerical analysis of binary solid–liquid phase change using a continuum model. *Numerical Heat Transfer*, 1988, **13,** 277–296.
13. Krane, M. J. M. and Incropera, F. P., A scaling analysis of the unidirectional solidification of a binary alloy. *International Journal of Heat and Mass Transfer*, 1996, **39,** 3567–3579.
14. Krane, M. J. M. and Incropera, F. P., Analysis of the effect of shrinkage on macrosegregation in alloy solidification. *Metallurgical and Materials Transactions A*, 1995, **26A,** 2329–2339.
15. Prince, A., *Alloy Phase Equilibria*. Elsevier, Amsterdam, 1966.
16. West, D. R. F., *Ternary Equilibrium Diagrams*, 2nd edn. Chapman and Hall, London, 1982.
17. Krane, M. J. M., Transport phenomena during the solidification of binary and ternary metal alloys. Ph.D. dissertation, School of Mechanical Engineering, Purdue University, West Lafayette, IN, 1996.